A Scalable Peak Shedding Solution for District Heating: Field Test, Simulation and Building Typology Analysis

Reza Mokhtari[a,], Jan Eric Thorsen[b], Rongling Li[a]

[a] *Technical University of Denmark, Department of Civil and Mechanical Engineering, Kgs. Lyngby, Denmark*
[b] *Danfoss District Energy, DK-6430 Nordborg, Denmark*

Abstract

In recent years, district heating has been undergoing a systematic transition to low-temperature networks to support green transition and decarbonization goals. Meanwhile, peak demand remains an unsolved operational challenge, causing high reliance on fossil-fuel boilers and other operational issues. At the building level, large peaks are often caused by Domestic Hot Water (DHW) tank charging. Demand response is a widely studied and known solution for managing peaks but existing solutions are mostly external signal-based and require dynamic tariffs, forecasting, and communication infrastructure that most district heating substations lack. This paper presents a physics-based, easily implementable peak shedding strategy called DHW Peak Compensation (DHWPC), in which tank charging itself triggers a short, autonomous interruption of the space heating supply. The strategy was field tested in a Danish multi-family building over 51 days, covering 228 DHWPC events. The measured peak substation demand and flow fell by 33% and 39%, respectively, although the building consumed 8.5 % more energy due to rebound effect. Measurements of the experiment showed that no apartment exceeded the ±1 K comfort band. The strategy was applied to a district scale with 50 buildings in simulation, and results show the reduction of the district peak demand by 32% and flow by 17%. Further analyses showed that the peak load reduction potential of the strategy relies on the tank size, DHW tapping, flow rate in the DHW charging circuit, and the ratio between space heating and DHW demand of the building.

Keywords: District Heating, Peak shedding, Domestic Hot Water, Demand

Preprint not peer reviewed

This preprint research paper has not been peer reviewed. Electronic copy available at: https://ssrn.com/abstract=7648871

Nomenclature

Abbreviations

CV-RMSE	Coefficient of variation of the root mean squared error
DH	District heating
DHW	Domestic hot water
DHWPC	Domestic hot water peak compensation
DR	Demand response
DSM	Demand side management
FMU	Functional Mock-up Unit
HDD	Heating degree days
KPI	Key performance indicator
MAE	Mean absolute error
NMBE	Normalised mean bias error
PI	Proportional–integral (controller)
RMSE	Root mean squared error
SH	Space heating

Symbols

Symbol	**Description**	**Unit**
E_{DH}	Total substation heat energy delivered over a period	MWh
E_{DHW}	DHW energy, incl. tapping and circulation losses	MWh
E_{SH}	SH energy	MWh
$E^{\mathrm{norm}}_{\mathrm{SH},2026}$	SH energy in 2026 normalised to 2025 weather	MWh
E_{shed}	Shed energy of an event	kWh
E_{reb}	Rebound energy of an event	kWh
f_{DHW}	DHW demand ratio	%
HDD_d, HDD	Daily and cumulative heating degree days	K d
N	Number of days in the comparison period	–
n	Number of samples in the validation period	–
$P^{k}_{\mathrm{SH}}(t)$	Measured SH power on the k-th reference day	kW
$P^{\mathrm{raw}}_{\mathrm{SH,baseline}}(t)$	Raw Y-day SH baseline	kW
$P_{\mathrm{SH,baseline}}(t)$	Corrected SH baseline	kW
$\bar{P}_{\mathrm{SH,pre}}$	Mean measured SH power in the pre-event window	kW
$P_{\mathrm{DHWPC}}(t)$	Measured SH power under DHWPC	kW

Preprint not peer reviewed

This preprint research paper has not been peer reviewed. Electronic copy available at: https://ssrn.com/abstract=7648871

P_{shed}	Maximum shed power of an event	kW
P_{reb}	Maximum rebound overshoot above the baseline	kW
$P^{\text{total}}_{\text{baseline,peak}}$	Peak total heat demand in the reference case	kW
$P^{\text{total}}_{\text{DHWPC,peak}}$	Peak total heat demand under DHWPC	kW
P_{floor}	Demand floor set by DHW charging under DHWPC	kW
T_{amb}	Ambient temperature	C
T_{base}	Base temperature for heating degree days	C
T_{indoor}	Indoor air temperature	C
t_0	Event start time	min
$\dot{m}$	Total substation mass flow (simulation)	kg/s
Y	Number of reference days in the baseline	–
y_i, $\hat{y}_i$	Measured and simulated hourly-mean values	–
$\bar{y}_{\text{meas}}$	Mean measured value over the validation period	–
Greek symbols		
α	Baseline scaling factor	–
Δ_{event}	Event duration	min
Δ_{rec}	Recovery period	min
Δ_{reb}	Rebound period	min
ΔT_{indoor}	Indoor temperature deviation from event start	K
τ_{pre}	Pre-event window length	min
Indices		
d	Day	
i	Sample	
k	Reference day	

1. Introduction

District heating (DH) plays a central role in the decarbonisation of the heating sector [1]. While DH networks are gradually moving towards lower supply temperatures and are including larger shares of renewables and waste heat, the peak demand issue remains a challenge. In practice, the peak demand issue is often addressed by oversizing network components and plants in the design phase, leading to unnecessarily high costs and unused system capacity. In existing DH networks, peak demand issues are tackled by installing large heat storage facilities or additional heat production units [2].

Heat consumption is well-synchronised, and the coincident morning and evening peaks are often covered by carbon-intensive fossil fuel boilers. Frequent demand spikes also cause congestion in the transmission network and

Preprint not peer reviewed

This preprint research paper has not been peer reviewed. Electronic copy available at: https://ssrn.com/abstract=7648871

limit how far supply temperatures can be lowered. Peak demand issues at the building level are often a network dimensioning issue, and the literature offers two categories of solutions. On the supply side, thermal storage units can absorb demand variations, but these solutions are often costly and are more suited to shifting heat from days to seasons rather than removing spikes that last only minutes or hours [3]. On the demand side, however, peak issues can be handled individually by reducing a building's own peak demand. Demand response (DR) and demand side management (DSM), the deliberate and temporary modulation of a building's heat demand, have become the main instruments for this purpose [4]. While most DR and DSM studies in DH-connected buildings typically target space heating systems, some studies use DHW as a flexibility source [5].

Existing studies show two peak shedding paradigms based on how an event is initiated [6]. In signal-based strategies, also known as demand response, the building adjusts its heat use in response to an external signal, most commonly a dynamic tariff, a marginal-cost signal, or a direct request from the network operator [4]. In physics-based peak shedding, the event is initiated by a locally observable physical condition inside the building substation, without reliance on any external signal. Signal-based strategies are by far the more studied paradigm, but with limited field tests. Christensen et al. [7] conducted a field test for a signal-based peak shedding strategy in 13 apartments in Copenhagen, Denmark connected to district heating network. They controlled room setpoints during peak hours and reported a 85% reduction in peak-hour energy consumption and minimal impact on the indoor temperature. Suhonen et al. [8] simulated rule-based, price-triggered SH DR for three building types in Finland and Germany and reported energy savings of 0.5-7.7% and cost savings of 0.7-8.1%, depending on building type, climate, and price volatility. Buffa et al. [9] demonstrated a neural-network-based model predictive controller in a fifth-generation DH network in simulation that shifted up to 14% of a substation's peak electricity consumption to off-peak hours, at the cost of a 4% drop in heat pump efficiency. Ju et al. [10] conducted a simulation study where they combined SH DR with a 500 m^3 thermal storage tank in Espoo, Finland, under dynamic marginal-cost pricing, saving 12.8% in energy costs and allowing a 43% reduction of the peak power limit without compromising comfort. The spatial level of control also matters. Zokirov [11] reports an energy saving potential of up to 15% for centralized building-level control. Mokhtari et al. [12] conducted an experimental analysis in which they implemented a price-based reinforce-

Preprint not peer reviewed

This preprint research paper has not been peer reviewed. Electronic copy available at: https://ssrn.com/abstract=7648871

ment learning controller as the local building controller for a dormitory's indoor thermostat in the NEST living lab in Switzerland. They reported a cost saving of 79% compared to the default rule-based controller. These studies establish that signal-based strategies in DH buildings are technically feasible and comfort-preserving but require communication infrastructure, price or load forecasting, and complicated controllers, which together limit the scalability of such solutions.

Physics-based peak shedding, on the other hand, utilizes real-time thermohydraulic measurements inside the building substation to initiate load shedding autonomously, and can therefore be implemented in existing substation control hardware. Autonomous, hardware-level, field-validated peak shedding mechanisms are under-represented [13, 14]. Such control solutions can fill the current gap and scale easily due to their simplicity, an advantage that remains largely unexplored.

This paper addresses this gap through a field test and a district scale simulation study. We present Domestic Hot Water Peak Compensation (DHWPC) control logic, which is designed to temporarily switch off the SH loop when the DHW tank in the building is charging. In other words, the charging of the DHW buffer tank is taken as a physics-based trigger for SH load shedding, and whenever the tank starts charging, the SH supply is temporarily paused. The method is tested in a multi-family residential building of 45 flats in Sønderborg, Denmark, comprising for 51 days during February - April 2026. Afterwards, simulation studies are conducted to investigate the impact of the method on the district level for a district of 50 large residential buildings.

The remainder of the paper is organised as follows. Section 2 describes the methodology, including the experimental setup, the baseline construction, the KPI definitions, and the simulation framework. Section 3 presents the field test results, rebound analysis, and peak load reduction, and Section 4 presents the simulation findings of district-level study and the typology analysis. Section 5 discusses the main findings and limitations of the work. Finally, Section 6 presents the conclusions and outlines directions for future work.

Preprint not peer reviewed

This preprint research paper has not been peer reviewed. Electronic copy available at: https://ssrn.com/abstract=7648871

2. Methodology

2.1. DHWPC strategy

The logic behind this strategy is to compensate the heat demand spikes of the building caused by DHW tank charging by turning off the SH demand. Since the DHW tank charging usually has a duration in the order of minutes (but can also be longer depending on the system design), it is expected that the SH interruptions would be mitigated by the thermal mass of the system thus no significant room temperature decrease. The triggering parameter for the DHW operation status is the measured water flow in the secondary side of the DHW loop, where a non-zero value denotes a DHW tank charging demand. In practice, this signal is used to detect DHW demand and overwrite the forward temperature setpoint of the SH loop to forcefully turn off the valve in the primary side of the SH loop. This process continues until DHW tank charging stops. The heating setpoint in the SH loop is then reverted to its original setpoint, based on the weather compensation curve.

2.2. Field test

The pilot building is a residential multi-family building encompassing 45 flats located in Sønderborg, Denmark. A detailed description of the building and network models can be found in [15]. The simplified heating diagram of the substation can be seen in Figure 1.

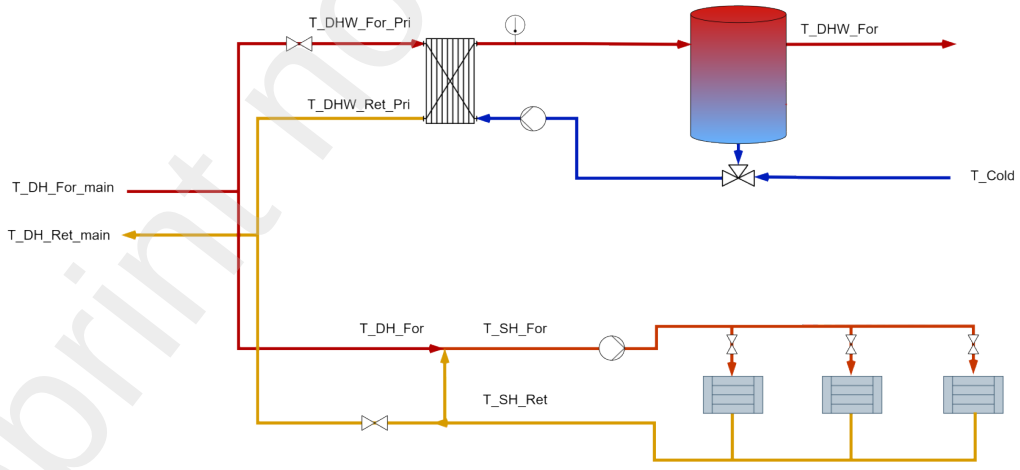


Figure 1: Simplified diagram of the heat substation in the pilot building, separated into space heating and DHW loops.

Preprint not peer reviewed

This preprint research paper has not been peer reviewed. Electronic copy available at: https://ssrn.com/abstract=7648871

The primary and secondary loops are separated by a plate heat exchanger for DHW charging loop and a mixing shunt in the SH loop. The DHW loop is equipped with a 500 L buffer tank. The DHW circulation loop is heated by an external heat exchanger that is removed from the diagram for simplicity. The DHW loop is operated based on the temperature sensor at the top of the tank, where the charging starts when the tank top temperature drops to 50°C and stops when the top temperature reaches 53°C. The historical measurement data indicate that the tank charging normally occurs 4-6 times a day, each lasting between 12 and 18 minutes. The charging frequencies and durations depend on the tank size, tapping amount, and the flow rate in the charging loop. To test the impact of the flow in the DHW charging loop, the experiment is conducted in two phases, with different flow rates, and the findings are compared. The DHWPC strategy was implemented through Leanheat® Monitor portal [16], which is the substation control platform. The building heat measurements are logged every minute and the indoor temperature sensors, placed in 40 flats, are logged every 5 minutes.

2.3. Large-scale simulation to examine DHWPC's grid impact

To examine the aggregated impacts of the DHWPC on the district heating network, a simulation study is conducted. The simulation model of a neighborhood consisting of 50 residential buildings based on the pilot building is created in Modelica, including building thermal zones, DHW tank, the SH radiator circuit, and the heat substation. MixedAir component from the Modelica Buildings Library is used to create the building thermal zones [15]. The model is compiled to a Functional Mock-up Unit (FMU) and co-simulated in Python using the fmpy library, building on the Modelica Buildings Library developed by LBNL [17]. The simulation interval is set to 1 minute to match the measurements, using DASSL as the solver with tolerance of 0.0001. The buildings in the simulated neighborhood are the same as the pilot test building. For diversification, each building is assigned a daily DHW profile drawn randomly from the measured DHW tank charging data of the pilot building. Each daily profile consists of several tank charging cycles. To represent the coincidence of DHW use during morning and evening peak hours, one charging cycle of each building is shifted to a common morning time period of 06:00 - 09:00 and evening time 17:00 - 21:00. A stochastic variation of normally distributed with standard deviation of 5 min is added to these times for each building to account for the different tapping timing and the stochasticity of DHW tank charging timing. The

Preprint not peer reviewed

This preprint research paper has not been peer reviewed. Electronic copy available at: https://ssrn.com/abstract=7648871

district is simulated over one week in winter in DHWPC mode, and the results are compared with the reference mode, using the same DHW profiles in both modes. The impacts of the DHWPC on the district in terms of peak demand, peak flow in the network, and comfort conditions are then analyzed.

2.4. Analysis of DHWPC strategy on different building typologies

The DHW demand ratio f_{DHW} is defined as the ratio of DHW energy consumption to the total substation heat consumption (Eq. 1), expressed in percentage, and serves as a building typology parameter. Low energy buildings normally have higher f_{DHW} and buildings with poor thermal insulation typically have lower f_{DHW}.

$$f_{\mathrm{DHW}} = \frac{E_{\mathrm{DHW}}}{E_{\mathrm{DH}}} \times 100 \tag{1}$$

where E_{DH} is the total substation heat energy delivered over the period and E_{DHW} is the total DHW demand, i.e., including both tapping demand and circulation losses [18]. For the pilot building, f_{DHW} is computed over the full year measurement data in 2025. The resulting value is $f_{\mathrm{DHW}} = 29.8\,\%$.

To assess the effectiveness of the DHWPC strategy in different building types, three building typologies are selected based on f_{DHW}, including 16 % as the reported value for EU28 average households in 2013 [19] and 45 % for representing energy-efficient buildings, that is reported to be between 40% - 50% [20].

The different building typologies were represented by modifying the heat demand profile to achieve the target annual f_{DHW}. This was done by scaling the annual space heating demand using a multiplicative factor, while leaving the measured DHW demand unchanged. Consequently, the temporal profile and timing of DHW consumption were preserved, whereas the magnitude of the space heating demand was adjusted. This approach is based on the assumption that differences between building typologies are primarily reflected in their space heating demand, while DHW consumption is mainly driven by occupant behaviour and occupancy patterns and is assumed to be similar among the building types. A parametric study is then conducted using Modelica model of the building, wrapped as FMU and simulated by Python to assess the relationship between f_{DHW} and the peak load reduction potential by DHWPC strategy. The simulation timestep was set to 1 minute to match the measurement data interval for comparison.

Preprint not peer reviewed

This preprint research paper has not been peer reviewed. Electronic copy available at: https://ssrn.com/abstract=7648871

2.5. Evaluation methods and KPIs

2.5.1. DHWPC event evaluation

To analyse the impact of the DHWPC mode and compare different cases, relevant KPIs are defined to characterise the SH load curve, which align with the canonical framework of the IEA EBC Annex 67 [21] and are illustrated in Figure 2.

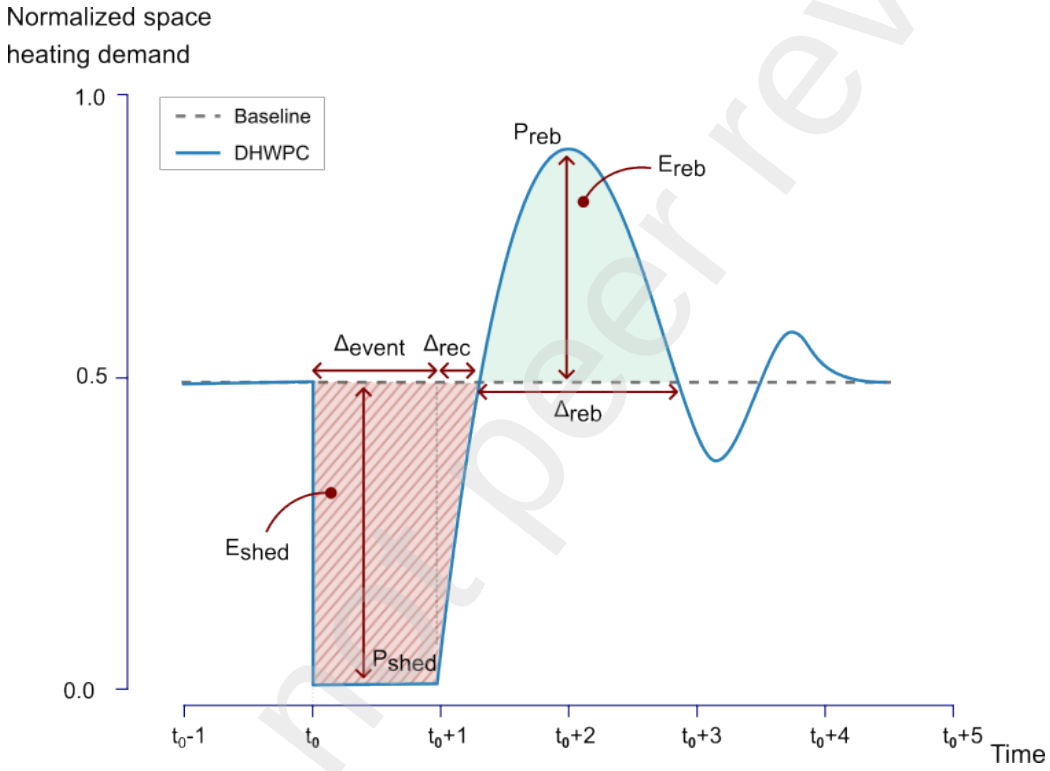


Figure 2: A SH demand profile in DHWPC mode, annotated with flexibility characterizing parameters.

Figure 2 illustrates a schematic SH demand profile for the DHWPC mode comparing with the baseline operation.

Baseline definition

In the baseline operation the space heating system operates under normal, undisturbed conditions. The baseline is constructed using the *Y-day average* method, specified in [22]. For each event on date d, the baseline is defined as the element-wise mean of the $Y = 10$ most recent normal days of the same day

Preprint not peer reviewed

This preprint research paper has not been peer reviewed. Electronic copy available at: https://ssrn.com/abstract=7648871

type (weekday or weekend), scaled by a correction factor α derived from the 30 min pre-event demand window, to account for daily variation in ambient temperature and system state. Full detail of the baseline construction process is provided in Appendix A.

Shed and rebound energy

During an event, space heating demand is curtailed by a maximum amount of P_{shed} relative to the baseline with a duration of Δ_{event} (corresponding to the DHW tank charging duration). Once normal operation resumes, the SH load takes some time to fully recover, mainly due to the inertia of the heating system components. This period is called the recovery period Δ_{recovery}. The shed energy, E_{shed}, is accordingly defined as the reduced SH energy relative to the baseline, computed from the event start to the moment the load returns to the baseline value, i.e., over $\Delta_{\text{event}} + \Delta_{\text{rec}}$:

$$E_{\text{shed}} = \int_{t_0}^{t_0+\Delta_{\text{event}}+\Delta_{\text{rec}}} (P_{\text{baseline}}(t) - P_{\text{DHWPC}}(t))\,\mathrm{d}t \tag{2}$$

After the recovery, the SH demand typically overshoots the baseline by P_{reb}, as the control system tries to compensate for the reduced flow temperature in the system, as a result of shedding energy. This often causes overshoot of the heat demand if the control system parameters are not well-tuned for the system. This overshoot is known as the rebound effect, and it can potentially cause new peaks in the system.

Studies in the literature define the rebound period in different ways. Reynders et al. [23] define the rebound energy over the full post-event horizon, until the system fully returns to baseline, which is mostly feasible in simulation studies where the baseline is available indefinitely. Zhang and Kummert [24], instead, define the rebound energy over a fixed period after the event has finished. Since the present experiment involves several events per day occurring every few hours, neither approach for rebound energy identification is directly applicable. A full-horizon integration risks overlapping with the next event, while a fixed-duration window may not consistently capture the true rebound energy across events. We therefore define the rebound energy, E_{rebound}, as the summation of the excess SH demand between the DHWPC and baseline modes, starting once the demand has crossed back above the baseline (at $t_0 + \Delta_{\text{event}} + \Delta_{\text{rec}}$) and continuing for a duration of Δ_{reb}, until the measured demand first falls back to baseline:

Preprint not peer reviewed

This preprint research paper has not been peer reviewed. Electronic copy available at: https://ssrn.com/abstract=7648871

$$E_{\text{reb}} = \int_{t_0+\Delta_{\text{event}}+\Delta_{\text{rec}}}^{t_0+\Delta_{\text{event}}+\Delta_{\text{rec}}+\Delta_{\text{reb}}} (P_{\text{DHWPC}}(t) - P_{\text{baseline}}(t))\,\mathrm{d}t \tag{3}$$

Further oscillations beyond Δ_{reb} are considered as systematic fluctuations of the control system rather than part of the rebound response, and are excluded from the KPI calculation.

2.5.2. DHWPC Event selection and cleaning

Prior to KPI calculation, the detected events were cleaned to exclude cases with unreliable baseline or rebound estimations. An event was excluded if any of the following criteria were observed:

1. Insufficient data coverage in the pre-event or post-event window.
2. Fewer than 50 % of pre-event timesteps with active SH demand, indicating an unstable heating state prior to the event.
3. An event starting within 30 min after the rebound of the previous event has ended. The rebound end is identified as the moment at which the measured SH power returns to the baseline.

There are 259 events tested in total, of which 228 remain after applying the cleaning steps and their details are presented in the results section.

2.5.3. Thermal comfort metric

Since DHWPC events are short, their comfort impact is assessed as the deviation in indoor temperature relative to its value at event start, $\Delta T_{\text{indoor}}(t) = T_{\text{indoor}}(t) - T_{\text{indoor}}(t_0)$, over a 240 min window following the event start. An event is considered not violating thermal comfortable if $|\Delta T_{\text{indoor}}|$ remains within 1K.

2.5.4. Heating Degree Day for weather normalized comparison

To assess whether the DHWPC strategy has increased or reduced the building energy consumption during the experiment in 2026, it is compared with the heat consumption in the same experiment period but in 2025. However, since space heating demand depends strongly on outdoor conditions, a direct comparison between the experiment period in 2026 and 2025 could be biased by differences in weather. The heat consumption was therefore normalised using the heating degree day (HDD) method. For each day d,

Preprint not peer reviewed

This preprint research paper has not been peer reviewed. Electronic copy available at: https://ssrn.com/abstract=7648871

the heating degree days were calculated from the daily mean ambient temperature $\bar{T}_{\mathrm{amb},d}$ measured at the building as

$$\mathrm{HDD}_d = \max\left(0,\ T_{\mathrm{base}} - \bar{T}_{\mathrm{amb},d}\right), \qquad \mathrm{HDD} = \sum_{d=1}^{N} \mathrm{HDD}_d, \tag{4}$$

where T_{base} is the base temperature commonly used for degree day statistics, defined as the outdoor temperature above which no space heating is assumed to be required, set to 17°C in Denmark. The daily total heat energy was then calculated by integrating the measured one-minute heat power. The 2026 SH energy was normalised to the 2025 weather as

$$E^{\mathrm{norm}}_{\mathrm{SH},2026} = E_{\mathrm{SH},2026}\,\frac{\mathrm{HDD}_{2025}}{\mathrm{HDD}_{2026}} \tag{5}$$

2.5.5. KPI for simulation model validation

Model accuracy was assessed using the two calibration statistics specified in ASHRAE Guideline 14 [25], evaluated on hourly-aggregated data. The *Normalised Mean Bias Error* (NMBE) quantifies the systematic over- or under-prediction of the model relative to the mean measured value:

$$\mathrm{NMBE} = \frac{\sum_{i=1}^{n}\left(\hat{y}_i - y_i\right)}{n\ \bar{y}_{\mathrm{meas}}} \times 100 \quad (\%) \tag{6}$$

The *Coefficient of Variation of the Root Mean Squared Error* (CV-RMSE) quantifies the overall scatter of the model error relative to the mean measured value, penalising large instantaneous deviations more heavily than NMBE:

$$\mathrm{CV\text{-}RMSE} = \frac{1}{\bar{y}_{\mathrm{meas}}}\sqrt{\frac{1}{n}\sum_{i=1}^{n}\left(\hat{y}_i - y_i\right)^2} \times 100 \quad (\%) \tag{7}$$

where $\hat{y}_i$ is the hourly-mean simulated value, y_i the hourly-mean measured value, n the number of hourly samples, and $\bar{y}_{\mathrm{meas}}$ the mean of the measured signal over the validation period. The acceptance threshold for hourly data is $|\mathrm{NMBE}| < 10\,\%$, and CV-RMSE $< 30\,\%$ and a model satisfying both thresholds is considered adequately calibrated for energy performance simulation [25, 26].

Preprint not peer reviewed

This preprint research paper has not been peer reviewed. Electronic copy available at: https://ssrn.com/abstract=7648871

The indoor air temperature is validated using the Mean Absolute Error (MAE) and the Root Mean Squared Error (RMSE), both expressed in °C:

$$\mathrm{MAE} = \frac{1}{n}\sum_{i=1}^{n}\left|\hat{y}_i - y_i\right|, \tag{8}$$

$$\mathrm{RMSE} = \sqrt{\frac{1}{n}\sum_{i=1}^{n}\left(\hat{y}_i - y_i\right)^2}, \tag{9}$$

where $\hat{y}_i$ and y_i are the simulated and measured indoor air temperatures, respectively. MAE gives the average magnitude of the temperature error, while RMSE penalizes large deviations more heavily.

3. Pilot test results

This section presents the findings of the DHWPC field experiment, evaluated using the KPIs and baseline methodology defined in Section 2.

3.1. Overall evaluation of the testing period

The 1-minute data of SH demand, DHW demand and flow rates are used in assessing the system performance of the DHWPC strategy over the entire testing period (18 February - 9 April 2026). Figure 3 presents an overview of the experiment and its impact on the total demand of the building.

Preprint not peer reviewed

This preprint research paper has not been peer reviewed. Electronic copy available at: https://ssrn.com/abstract=7648871

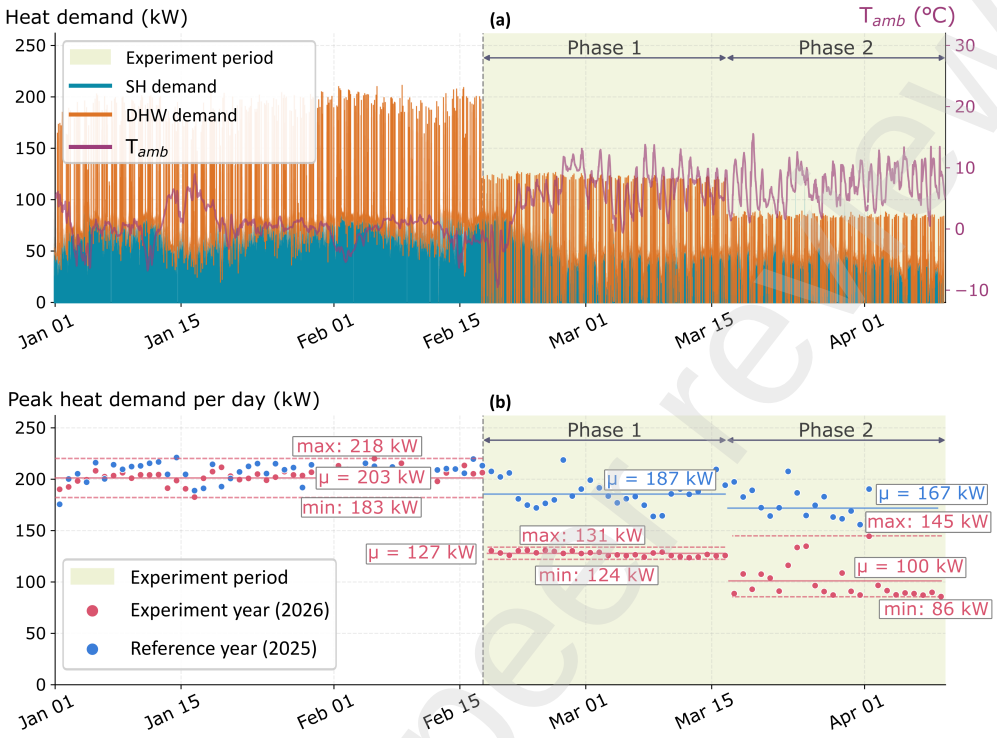


Figure 3: Impact of the DHWPC mode on the building heat load. a) Comparison of the pre-experiment and experiment periods including experiment phase 1 and phase 2, b) comparison of the peak heat demand per day prior to and during experiment period.

Figure 3.a shows the total building heat demand together with the ambient temperature (T_{amb}), covering both the pre-experiment period and the experiment period. The event period is divided into two phases corresponding to different DHW loop pump flow rates. In Phase 1, the pump operated at 42 L/min, resulting in DHW charging periods of approximately 11 min per event. From 2026-03-16 onward (Phase 2), the flow rate was reduced to 28 L/min, extending the charging duration up to 18 minutes while reducing the peak demand associated with each charging event.

As shown in Figure 3.a, both the average heat demand and the magnitude of demand peaks decrease in the experiment period. The magnitude of the peak reduction differs between Phases 1 and 2, reflecting the effect of reducing the DHW charging flow rate. The apparent demand ceiling on the reduced demand in the experiment period is caused by the DHW charging loop, since SH is off in the experiment period.

Preprint not peer reviewed

This preprint research paper has not been peer reviewed. Electronic copy available at: https://ssrn.com/abstract=7648871

To evaluate the peak load reduction, peak load is defined as the maximum building heat demand occurring each day. Accordingly, Figure 3.b shows the highest demand of every day (daily peak demand) during the experiment year and the reference year (2025). Before the experiments, the daily peak demand averaged 203 kW (range 183-218 kW). With DHWPC operated in Phase 1, the average daily peak dropped by 37% to 127 kW and stayed within a narrow band of 124-131 kW. Phase 2 reduced it by a further 22% to 100 kW (range 86-145 kW), about 51% below the pre-event level. Part of this reduction is due to the warmer weather in spring, which lowers the space heating demand. Compared with the same calendar days of the reference year (2025), the average daily peak was 32% lower in Phase 1 and 40% lower in Phase 2. As the weather gets warmer, the share of DHW in the total demand increases, and the daily peak under DHWPC is increasingly impacted by the DHW demand rather than by space heating.

To analyze the impact of DHWPC on the building and compare it with the normal operation, the experiment period (i.e., 18 February - 9 April) in 2026, was compared with the same period in 2025 as the reference year. To ensure a fair comparison and decouple the impact of weather, the derived energy consumption values are weather-normalized. The findings are illustrated in Figure 4.

Figure. 4.a shows the two periods had very close weather conditions with the calculated HDDs of 532.8 and 529.3 HDD, respectively. Only the SH energy was assumed to be weather dependent, whereas domestic hot water (DHW) and distribution losses were not normalised. The measured raw SH energy increased from 41.5 MWh in 2025 to 45.4 MWh in 2026 (+9.4 %) and an 8% increase in the building's total energy demand as shown in Figure. 4.b. After weather normalisation, this becomes +10.1% for SH energy and +8.5% for the building total energy demand. This shows that the DHWPC strategy has increased the building heat consumption by 8.5% compared to reference year. Figure 4.c shows the different heat demand levels for the two periods. Accordingly, the experiment has reduced the maximum peak demand from 218 kW to 145 kW, a reduction of 33 % compared to the reference operation. According to Figure 3.a, however, the 145 kW peak in the experiment period occurs only in a single event at 2026-04-01 in Phase 2, and the rest of events have a peak demand of around 90 kW. The 99th percentile heat demand has also reduced by 27 %, indicating an overall reduction in top 1 % of the peaks in the building. On the other hand, the 95th percentile has increased by 9 % and the average demand in the experiment period has increased by 8 %

Preprint not peer reviewed

This preprint research paper has not been peer reviewed. Electronic copy available at: https://ssrn.com/abstract=7648871

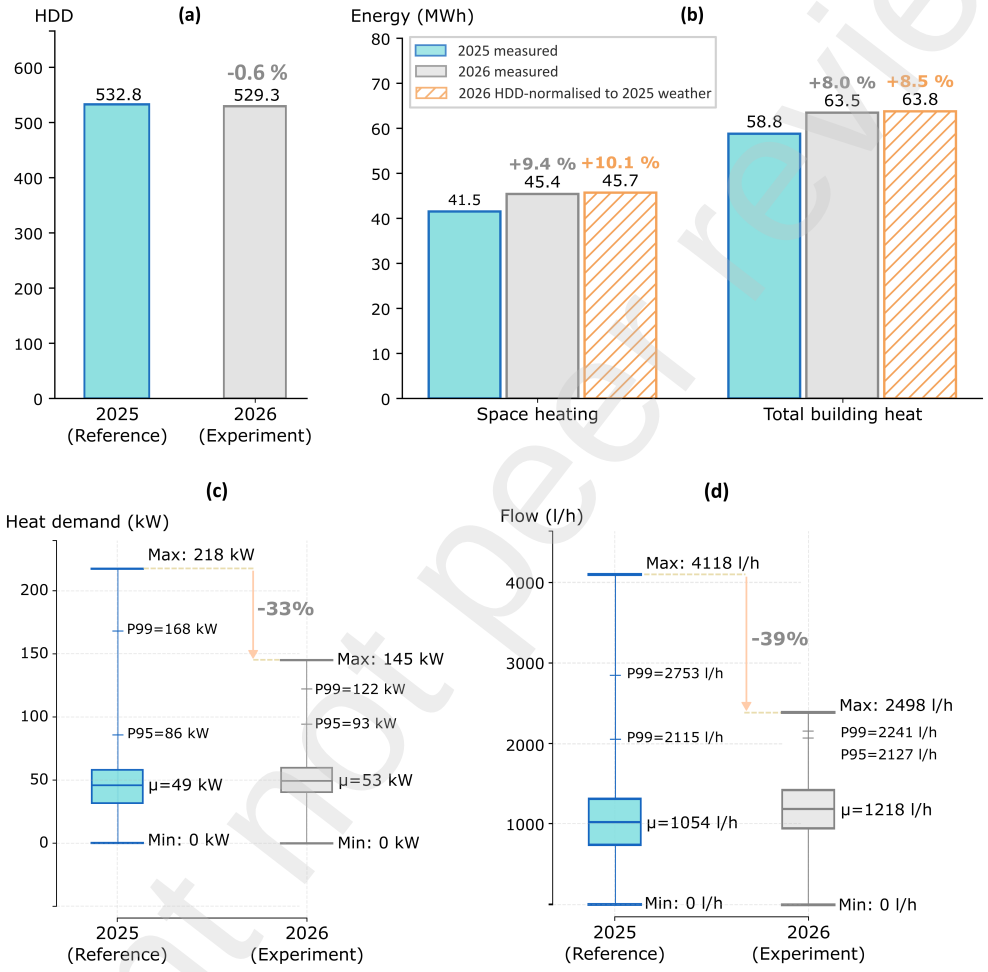


Figure 4: Comparison of the reference (2025) and DHWPC (2026) operation modes for the building from 18 February to 9 April, based on 1-minute measurement data. a) Calculated HDD based on measured ambient temperature, b) SH and total building heat energy, c) comparison of the building heat demand distribution and d) flow distribution.

Preprint not peer reviewed

This preprint research paper has not been peer reviewed. Electronic copy available at: https://ssrn.com/abstract=7648871

compared to the reference. Considering similar weather conditions between the two years, this increase is primarily due to rebound effect after the events, causing higher space heating supply to the building. The reduction in P99 and increase in the P95 indicate that the peaks are suppressed by DHWPC but the rebound effect distributes excess demand across a broader range of hours, shifting the P95 and the mean value higher. The peak flow of the building in the event period has been reduced by 39% applying DHWPC strategy, as shown in Figure 4.d. Accordingly, the average flow has also been reduced by 30%. The unlocked extra capacity by the DHWPC is both useful for buildings by reducing their capacity fees and for DH operators by solving their network congestion issues and enabling network extension.

3.2. Heat demand profiles of DHWPC events

Following the cleaning procedure described in Section 2.5.2, 228 events were retained. A summary of all events with their flexibility characteristics is provided in Table 2 and histograms of the parameters are shown in Figure 5.

Table 2: Summary of flexibility characteristics of the 228 events.

Event	T_{amb} (°C)	Δ_{event} (min)	Δ_{rec} (min)	Δ_{reb} (min)	E_{shed} (kWh)	E_{reb} (kWh)	P_{shed} (kW)	P_{reb} (kW)
1	−0.4	13	7	52	20.3	8.5	78.7	21.7
2	−1.9	12	6	94	20.2	10.2	82.3	13.1
3	−1.9	12	5	86	18.5	9.0	83.2	12.2
4	−3.1	16	5	68	23.3	13.6	84.0	20.3
5	−3.1	13	8	47	21.5	11.0	80.7	25.7
6	−0.4	13	4	31	9.8	22.1	46.5	51.3
7	−2.4	13	6	69	20.4	11.2	81.1	15.8
8	−6.0	14	5	360	22.5	56.4	84.6	17.0
9	−9.5	12	5	72	20.1	8.9	87.5	15.7
10	−7.9	13	13	61	22.8	9.0	90.6	15.7
...								
228	9.9	19	10	32	9.6	2.4	28.2	7.8
Mean	6.7	16.3	7.9	57.2	13.0	14.1	44.6	29.8
STD	3.8	14.1	4.2	53.4	8.2	10.5	16.6	17.0

Preprint not peer reviewed

This preprint research paper has not been peer reviewed. Electronic copy available at: https://ssrn.com/abstract=7648871

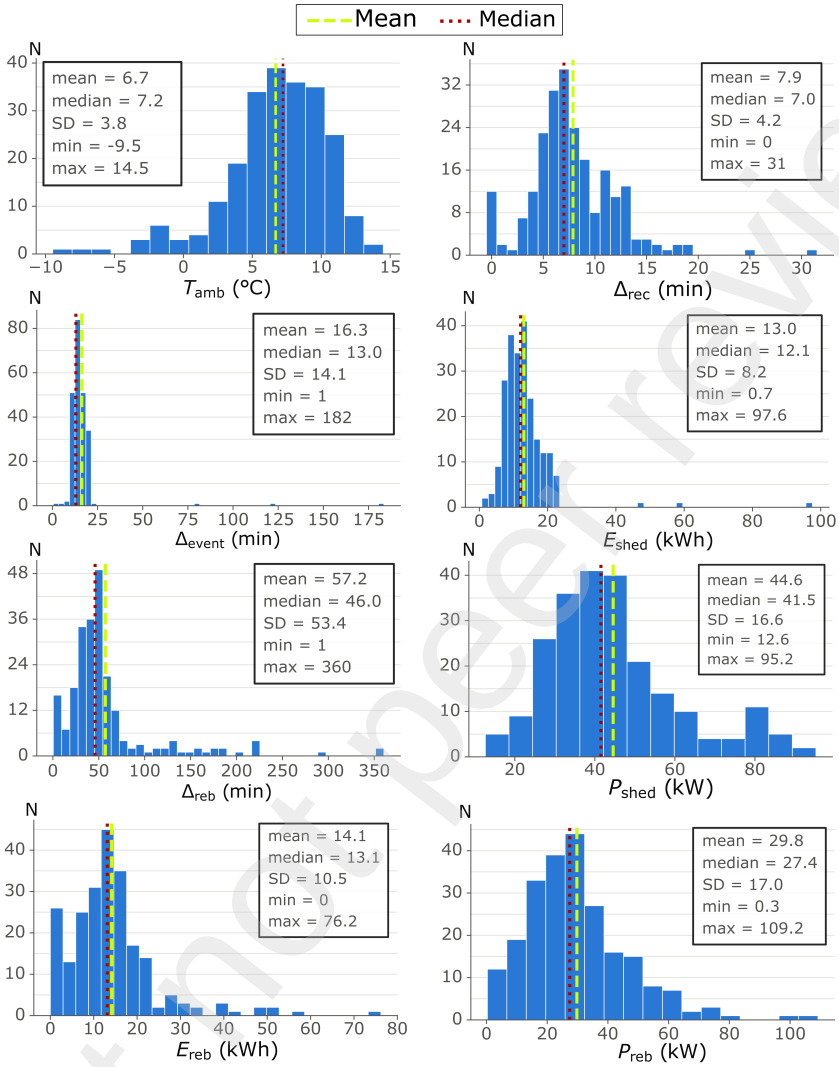


Figure 5: Histogram of flexibility characteristics of the 228 DHWPC events.

The higher mean and the substantially larger standard deviation of E_{reb} compared to E_{shed} indicates that the rebound response is more volatile than the shedding and, on average, larger in magnitude.

Dividing the total E_{reb} by the total E_{shed} throughout the entire events results in $\sum_i E_{\text{reb},i} / \sum_i E_{\text{shed},i} = 1.08$ that indicates about 8% more energy was consumed in rebound than energy shed throughout the whole experiment. DHWPC therefore primarily shifts space heating demand in time,

Preprint not peer reviewed

This preprint research paper has not been peer reviewed. Electronic copy available at: https://ssrn.com/abstract=7648871

with a slight net energy penalty. This is consistent with the literature on thermal DR, where SH load shedding is known to induce a compensatory rebound that can partially or fully offset the shed energy [27, 28], and with the increase in SH consumption reported in Figure 4.

Events last 16 minutes on average and the rebound usually lasts around 57 minutes, with a standard deviation of 53 minutes. This highlights the complexity of rebound, as it depends on dynamics of the heating system actuators, controller response speed, and the building dynamics. According to the summary table, it takes on average 8 minutes for the system to recover from the event, mainly due to the inertia of the control valve and setting of the PI control parameters, controlling the flow in the substation.

Figure 6 illustrates the heat demand response to the DHWPC strategy for four representative events.

Preprint not peer reviewed

This preprint research paper has not been peer reviewed. Electronic copy available at: https://ssrn.com/abstract=7648871

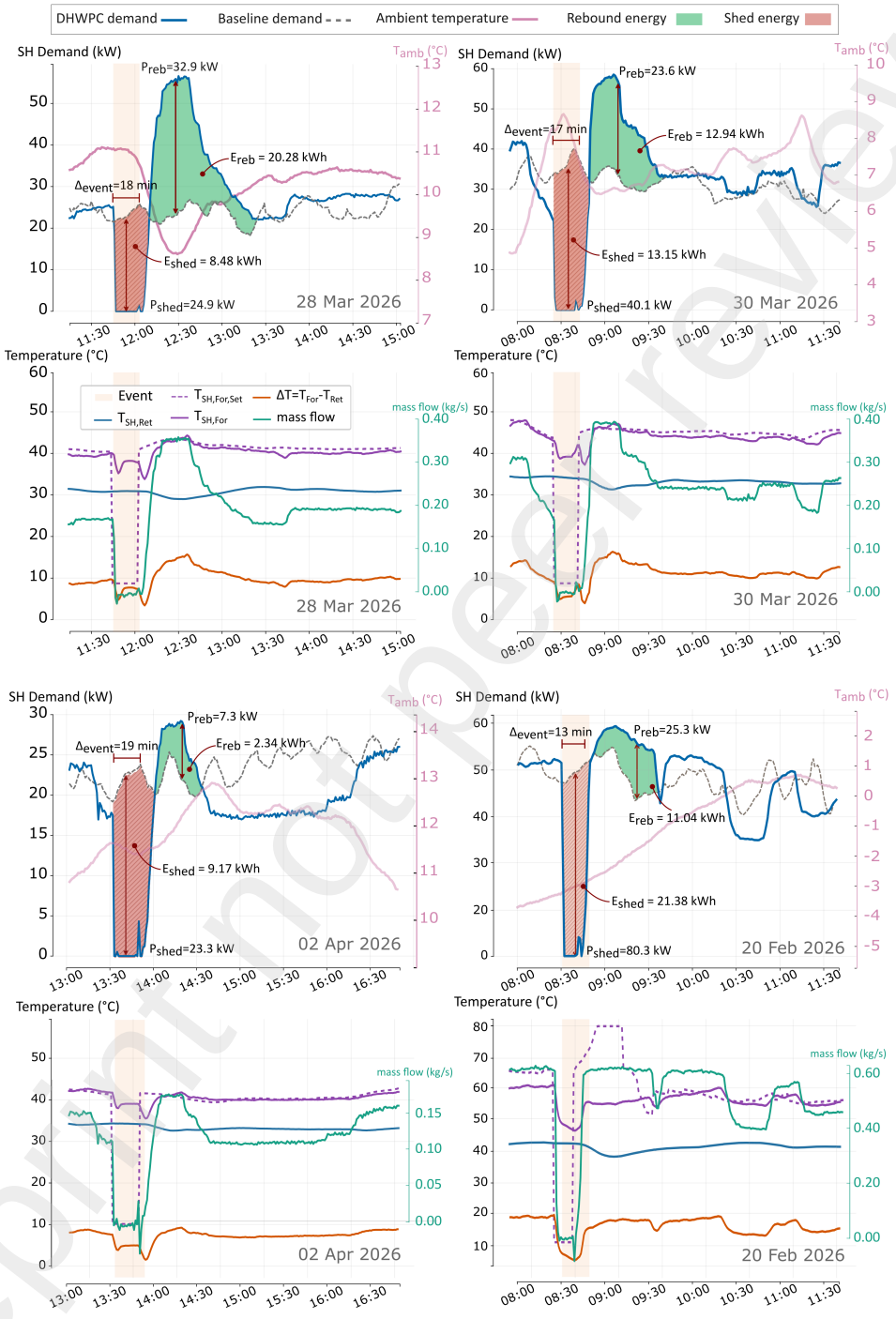


Figure 6: SH demand profile and substation conditions of four representative events. For each event, flexibility characteristics are presented, followed by substation sensor values.

Preprint not peer reviewed

This preprint research paper has not been peer reviewed. Electronic copy available at: https://ssrn.com/abstract=7648871

Figure 6 shows that the shedding power (P_{shed}) is higher when ambient temperature is lower, as the colder days have higher heating load. The shedding energy depends both on the event duration and ambient temperature. On the other hand, the rebound power and energy do not show any clear correlation with ambient temperature and event duration. After each event, the return and forward temperatures increase after a notable delay, caused by thermal inertia of the pipe and flow, temperature sensor placed on the pipe surface, and the controller response speed. The measurements show that after each event, flow increases suddenly due to the valves opening fully for the supply water to reach the setpoint. The diagrams indicate that the demand is mostly governed by the measured flow. Therefore, the rebound is caused by the controller providing high flow after each event. The rebound amount, thus, depends on how much the flow increases after the event. On 20 February 2026, although the flow temperature setpoint has increased after the event, flow has not increased compared to its pre-event value, due to the hydraulic limitation of the heating system. Therefore, although it is a comparatively cold day, lower rebound energy and power are observed after the event. Figure 7 shows the correlation between the flow change in SH loop and the P_{reb} for all the DHWPC events. $\Delta\dot{m}$ is calculated as the mass flow change at the time of peak rebound in relation to the mass flow at the time before the DHWPC event.

Preprint not peer reviewed

This preprint research paper has not been peer reviewed. Electronic copy available at: https://ssrn.com/abstract=7648871

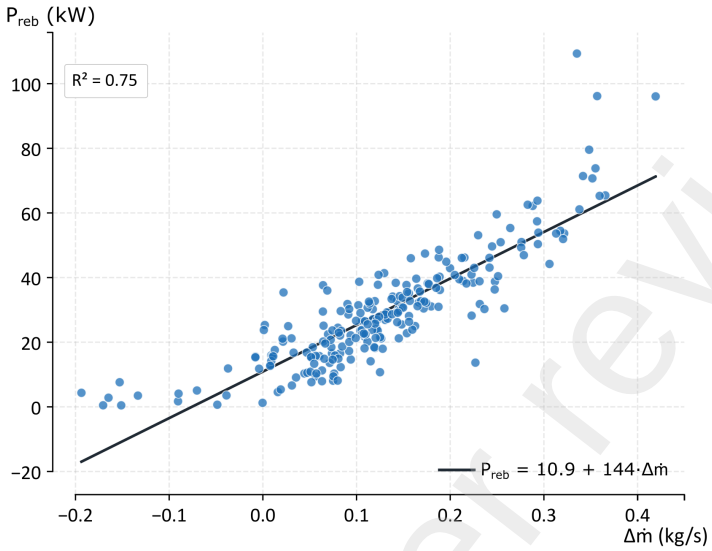


Figure 7: Correlation between P_{reb} and changes in mass flow in the SH loop after each event ($\Delta\dot{m}$), for the DHWPC events.

Figure 7 shows a strong positive correlation between P_{reb} and $\Delta\dot{m}$ across the events with $R^2 = 0.75$. The events with small deviation in flow show a lower rebound, whereas the highest rebounds appear at the highest flow changes. This indicates that the rebound peak is mainly a result of SH flow increase, that is caused by the controller overreaction after the events. Gradual increase of the flow after the events can reduce the rebound peak caused by the controller.

3.3. Thermal comfort assessment

This section shows the indoor temperature response to events, both at the building level and across the individual monitored apartments. Figure 8 presents the indoor temperature response to the events. Each profile is normalized by subtracting the indoor temperature at event start.

Preprint not peer reviewed

This preprint research paper has not been peer reviewed. Electronic copy available at: https://ssrn.com/abstract=7648871

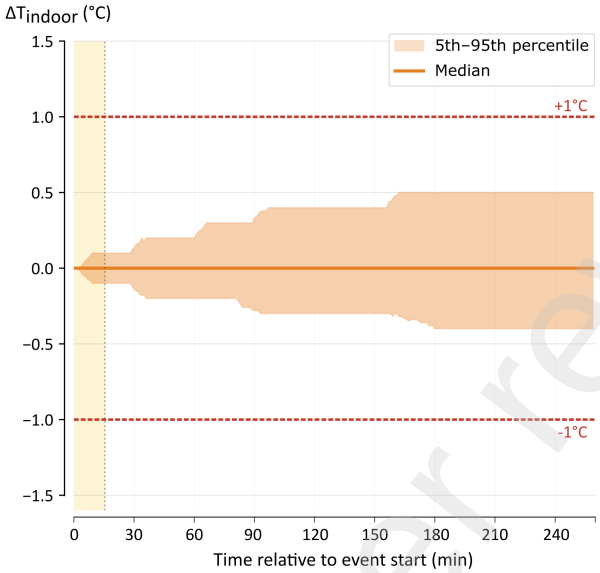


Figure 8: Per-apartment indoor temperature deviation across all 40×228 apartment-event combinations, expressed as the deviation from the indoor temperature at the moment of event start. The orange band shows the 5th-95th percentile range and the solid line shows the median. The yellow shading shows the mean event window ($\bar{\Delta} = 16$ min), and the red dashed lines indicate the ± 1 °C deviation.

Figure 8 shows the indoor temperature deviation $\Delta T_{\text{indoor}}(t) = T_{\text{indoor}}(t) - T_{\text{indoor}}(t_0)$ across all 40×228 apartment-event combinations (indoor temperature data was available for 40 out of 45 flats). The median deviation remains at 0 °C throughout the entire observation window. The 5th-95th percentile band widens gradually in the post-event window. A slightly positive asymmetry can be seen in this widening as the upper bound of the outer band extends marginally further than the lower bound, consistent with the post-event thermal rebound observed in Figure 4. Accordingly, when the controller resumes space heating operation after the event, some apartments have a small temperature increase and increased heat demand. The deviations remain within the EN 16798-1:2019 Category I comfort bound of ± 1 °C and no individual apartment exceeds the bounds at any point, consistent with the benchmark reported by [29].

Figure 9 shows the impact of DHWPC events on indoor temperature of apartments in the four representative events shown in Figure 6. The average temperature across all apartments is also plotted for each event. Mean ΔT is

Preprint not peer reviewed

This preprint research paper has not been peer reviewed. Electronic copy available at: https://ssrn.com/abstract=7648871

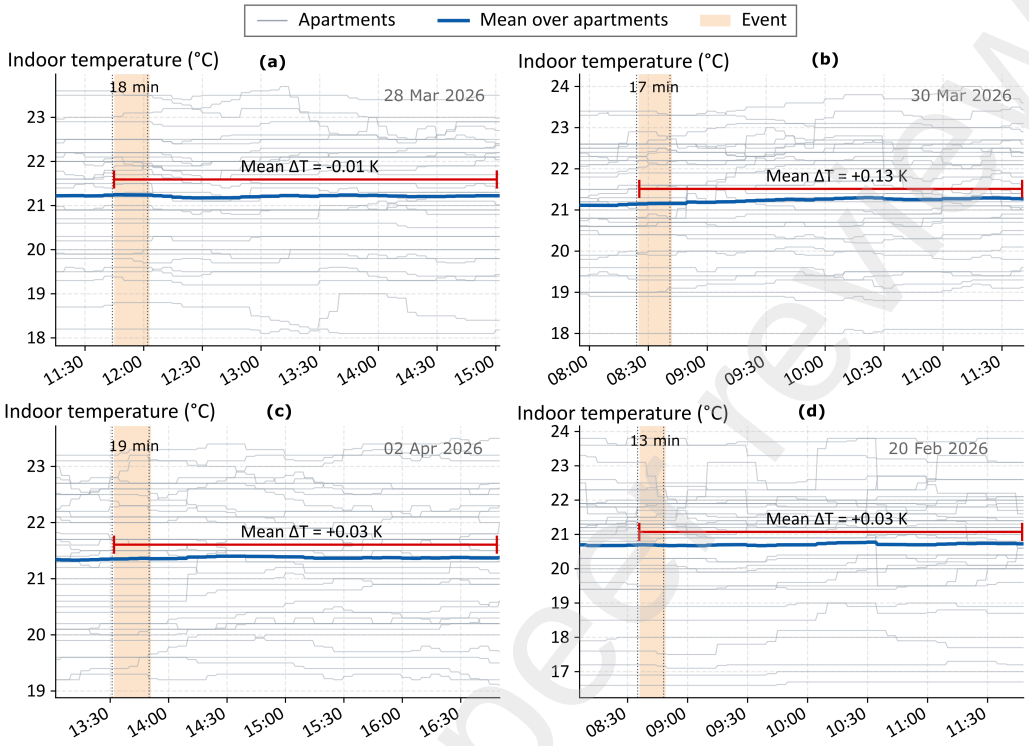


Figure 9: Impacts of the DHWPC on indoor temperature of apartments during and after the representative events described in Figure 6

calculated as the indoor temperature change between the event start and 180 minutes after the event started, averaged across all apartments. Accordingly, the temperature difference appears to be negligible with a maximum of +0.13 K. Individual apartments also does not show any clear temperature reduction or increase pattern during or after the events. This indicates that DHWPC has very little impact on the indoor conditions. The impact of turning off SH for longer durations can be seen in Appendix B.

4. District-level simulation results

This section presents the results of the simulation study, conducted to complement the field tests to investigate the impact of DHWPC strategy on DH network scale and to extend the evaluation of the DHWPC strategy across a broader range of building typologies than could not be tested experimentally.

Preprint not peer reviewed

This preprint research paper has not been peer reviewed. Electronic copy available at: https://ssrn.com/abstract=7648871

4.1. Model validation

The Modelica building model is validated against measured data from the building. The model reproduces the observed thermal behavior with sufficient accuracy. The validation results can be seen in Figure 10.

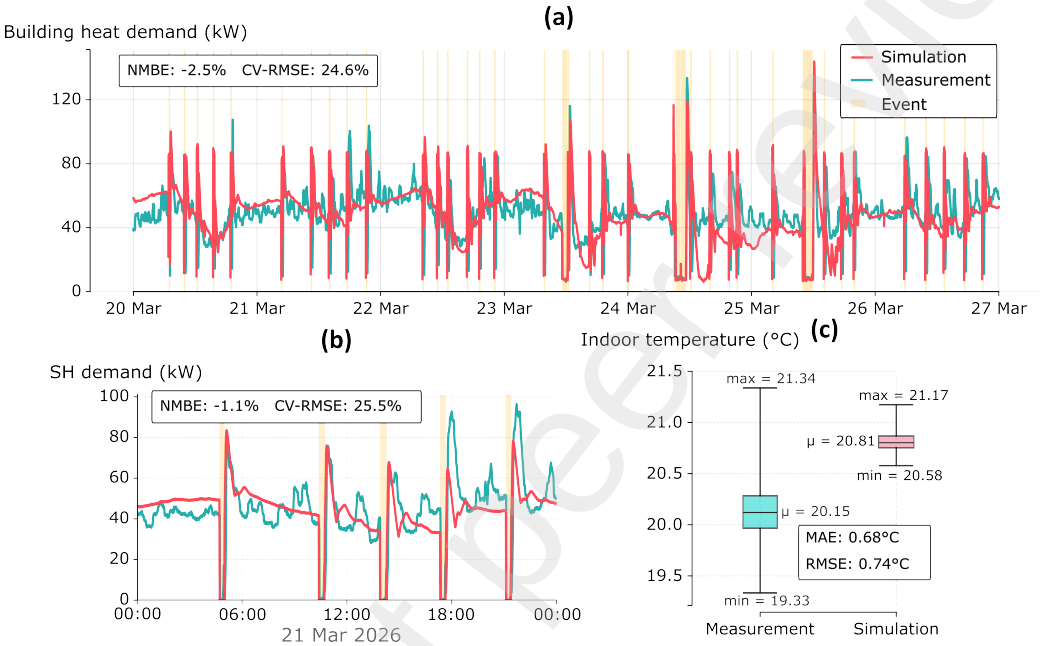


Figure 10: Validation results of the simulation model against sensor measurements. a) Building heat demand comparison, b) SH demand in a single day, and c) zone temperature comparison.

The validation period contains DHWPC events to analyze the simulation model behavior during and after events. Figure 10.b shows the SH demand behavior. The model has been calibrated to follow the measurement during and after events. Accordingly, the model shows similar SH demand behavior, but with fewer fluctuations due to unmodeled valve stroke behavior, controller fluctuations, etc. Figure 10.c shows the indoor temperature comparison distribution for the simulation and measurement. The simulation model shows a narrower spread, that is mainly due to the fact that the measurement is for average value across all apartments, but the simulation model is based on simplified thermal zone model, with lower fluctuations. However, the average temperatures match with 0.66°C difference between simulation and measurement. Overall, in all figures, CV-RMSE and NMBE values are

Preprint not peer reviewed

This preprint research paper has not been peer reviewed. Electronic copy available at: https://ssrn.com/abstract=7648871

all within the ASHRAE Guideline 14 thresholds, and MAE and RMSE values for indoor temperature are lower than 1°C, confirming that the Modelica model is adequately calibrated (Section 4.2).

4.2. District-level peak reduction

The calibrated building model is scaled to a district of 50 buildings, as described in Section 2.3, to evaluate the aggregated impact of the DHWPC. The district is simulated over a one-week winter period. Figure 11 presents the results.

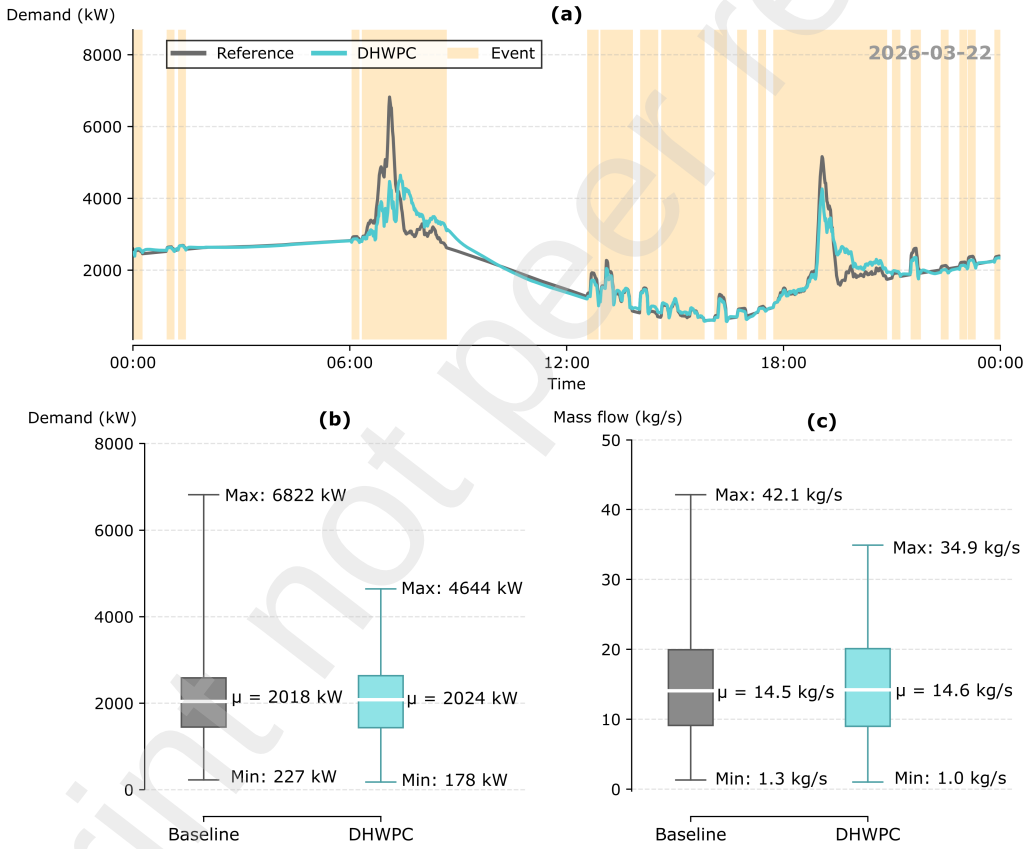


Figure 11: Comparison between reference and DHWPC modes for a district of 50 buildings. (a) Aggregated district heat demand in one representative day, (b) district heat demand distribution and (c) district mass flow distribution in 1-min interval.

Figure 11.a shows the aggregated heat demand time series over a single day of simulation period for both scenarios, with the reference demand

Preprint not peer reviewed

This preprint research paper has not been peer reviewed. Electronic copy available at: https://ssrn.com/abstract=7648871

and the DHWPC demand overlaid at 1-min resolution. According to the figure, the DHWPC operation mode cuts the demand peaks of the reference mode across every DHW charging event, while the two profiles remain closely aligned during off-peak periods. The charging events occur mostly around morning 06:00 - 09:00 and evening period of 19:00 - 21:00, with peak aggregated heat demand occurs mainly at 07:00 and 19:00. The rest of the charging events occur scatter throughout the day, with higher density in afternoons.

Figure 11.b illustrates the distribution of the aggregated district demand, where the maximum aggregated district demand falls from 6822 kW under the reference to 4644 kW under DHWPC mode, a reduction of 32 %, while the average district demand increases slightly from 2018 kW to 2024 kW. This is in line with the experiment findings, showing slightly higher energy consumption in DHWPC than reference.

Figure 11.c shows the distribution of district-level total substation mass flow, comparing the reference scenario against DHWPC operation. The maximum district flow decreased from 42.1 kg/s to 34.9 kg/s, a reduction of 17 %, while the mean flow did not change. This district-level reduction is notably smaller than the 39 % peak flow reduction measured for the individual pilot building (Fig. 4.d). This gap is due to the assumption in the simulation setup that building's DHW charging events occurs at different times, making the reduction at the aggregated level smaller than individual buildings.

These findings demonstrate that the DHWPC strategy can provide peak demand reduction on a large scale, in addition to individual building-level peak reduction, while preserving building thermal comfort, making it a practical, easy-to-implement demand-side peak reduction strategy for district heating utilities. This strategy is especially useful for reducing the peak demand and peak flow in the network during morning and evening peak hours.

4.3. DHWPC strategy effect on different building typologies

Three building typologies are simulated to assess the impact of the DHWPC strategy. Figure 12.a shows the monthly DHW ratio for each of the three cases over the heating period of Oct - April.

Figure 12.b shows peak load for both DHWPC and reference operation for EU28 average building. Both have a seasonal pattern, with a maximum peak reduction value of 31% occuring in January. Figure 12.c shows that the pilot building's peak loads in both modes are lower than the EU28 average building, and the peak reduction is highest in January with 32.6% reduction

Preprint not peer reviewed

This preprint research paper has not been peer reviewed. Electronic copy available at: https://ssrn.com/abstract=7648871

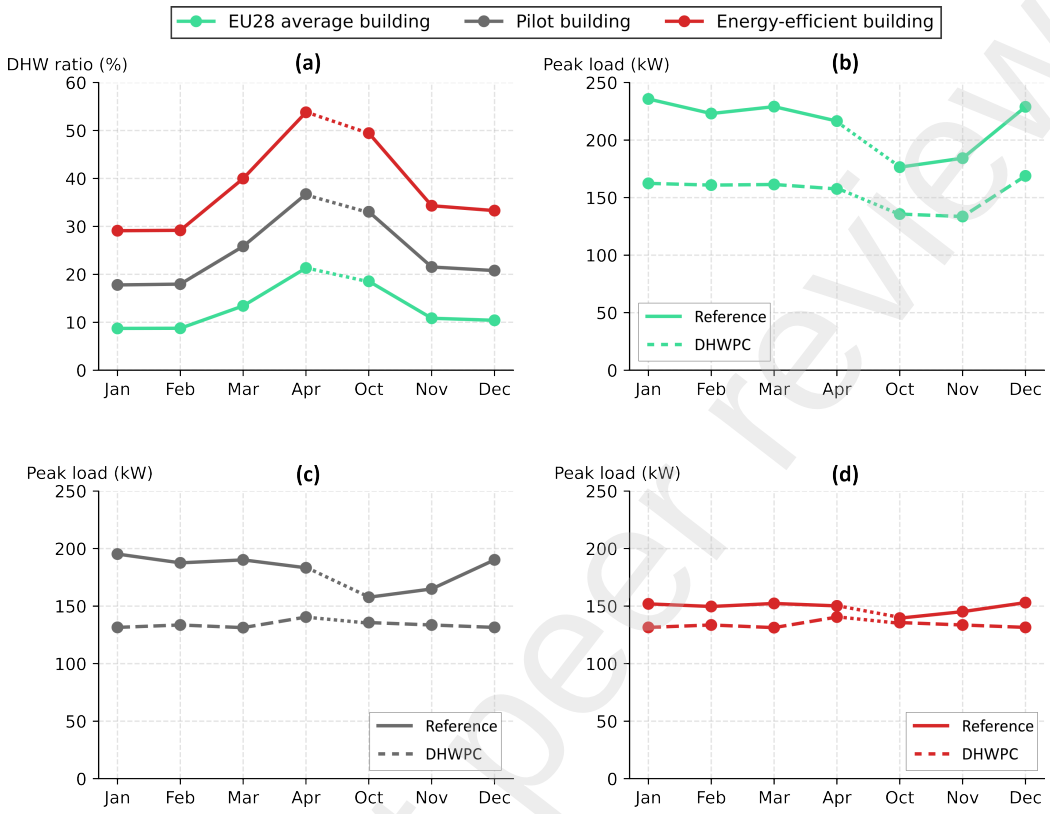


Figure 12: DHW ratio and corresponding peak load of the three building typologies simulated in 1-min resolution, under reference and DHWPC modes during heating period.

potential. Figure 12.d shows that the energy-efficient building has a lower peak load than the pilot and EU28 average buildings, with a maximum peak reduction occuring in December as 14%. The DHWPC peak load appears the same as the pilot building, indicating that the peak load in the energy-efficient building and pilot building are caused by the DHW charging demand. The peak caused by the DHW charging is primarily determined by the tank size and charging flow. At low f_{DHW}, DHWPC results in large P_{shed} and E_{shed}, but this reduction does not have a big impact on the large SH demand overal. At high f_{DHW}, on the other hand, the maximum reduction is limited by the magnitude of the DHW demand itself as the DHW charging demand becomes the dominant contribution to the building peak and therefore sets the limit on peak reduction with low P_{shed} and E_{shed}, this case also gives a low relative reduction on the heat demand. Accordingly, Figure 13 shows the

Preprint not peer reviewed

This preprint research paper has not been peer reviewed. Electronic copy available at: https://ssrn.com/abstract=7648871

relationship between the peak demand reduction and the DHW share of the building during the heating period, indicated in Figure 12.a. To generate the figure, the DHW demand of the building is kept fixed, and the SH demand is shifted to match DHW ratio values from 10% to 60%. Then the annual peak demand reduction is calculated for the highest peak throughout the year in DHWPC compared to reference.

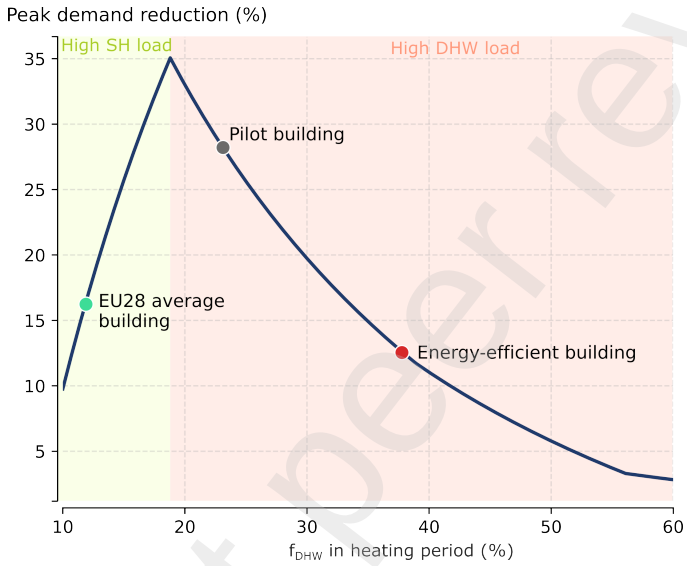


Figure 13: Reduction in annual peak heat demand achieved by DHWPC relative to the reference. Markers show the EU28 average building, the pilot building and an energy-efficient building. Shaded areas indicate the regime where the DHWPC peak. Reduction is limited by either DHW load or SH load dominating.

In the high SH load regime, the peak demand reduction starts with low values and increases with f_{DHW} until it reaches the peak, resulting in highest peak demand reduction. The primary cause of peak reduction limitation in this region is the rebound caused by the DHWPC events.

Beyond the sweet spot, the curve enters the high DHW load regime, where the remaining DHWPC peak is limited by the non-shiftable DHW demand, and further reductions in space heating no longer reduce the system peak. The relative peak reduction therefore declines as f_{DHW} increases further, since the reference peak continues to fall while the demand stays at the measured DHW demand.

The three building typologies lie on different areas of the curve, which explains the ordering of the reported peak reductions. The EU28 average

Preprint not peer reviewed

This preprint research paper has not been peer reviewed. Electronic copy available at: https://ssrn.com/abstract=7648871

typology sits on the Rebound-limited branch, where the daily peak remains space heating-dominated and DHWPC shaves a limited portion of the SH demand. The pilot building typology sits near the sweet spot. The energy-efficient building typology lies on the lower part of the DHW-limited regime where the peak is limited by the non-shiftable DHW demand.

This finding indicates that the buildings with higher peak reduction potential using DHWPC are those with a notable SH demand to shift, but whose DHW demand does not sit far below the SH peak. The case study building, despite being a relatively conventional Danish multi-family dwelling, is a suitable case for this strategy.

5. Discussion

5.1. Signal-based vs. physics-based peak shedding

Studies of peak shedding strategies are dominated by signal-based approaches, which require external signals such as price or CO_2 intensity signals [30, 8, 31]. The studied DHWPC strategy does not require any external signal for peak shedding. This means that no communication infrastructure, forecasting, or dynamic pricing is required, making it readily deployable, with a considerably higher technology readiness level than price-based DR and DSM requiring external direct control. DHWPC reduces the building's own peak demand significantly and has a clear impact on network-wide peak reduction.

DHWPC also requires no occupant engagement, and the results showed that room temperatures were not affected. However, the charging periods in this building were on average 16 minutes as shown in Table 2. A detailed study and field test on determining the maximum period over which SH can be turned off without endangering thermal comfort would extend the applicability of this work.

5.2. Generalisation of the approach

Although the DHWPC logic suggests that the approach can also be implemented in buildings with instantaneous DHW preparation, the method is best suited to buildings with a buffer tank for DHW tapping. Instantaneous DHW tappings create many small, short demand, for which DHWPC would trigger frequent short interruptions of the SH loop with only small peak reductions. Additionally, the reaction time of the heating system components is also often too slow to respond to short DHW tappings. DHW tanks, in

Preprint not peer reviewed

This preprint research paper has not been peer reviewed. Electronic copy available at: https://ssrn.com/abstract=7648871

contrast, usually cause larger charging peaks, making the method more effective for peak reduction. Handling the dynamics of the DHW storage tank is also an easier and more efficient task. For instantaneous DHW loops, one solution could be to reduce SH during high tapping periods such as during early mornings.

The results of the typology analysis on the DHW ratio indicated that the maximum peak load reduction achievable with DHWPC depends heavily on the DHW consumption relative to the total heat demand of the building. The high potential for peak load reduction belongs to buildings whose DHW ratio is higher than that of old, inefficient buildings, but lower than that of energy-efficient buildings. The proposed strategy therefore remains effective in a large share of building stock.

The replication of the method mainly requires an actuator on the SH main supply loop, a flow or heat meter in the DHW charging loop (or a signal indicating DHW tank charging), a DHW tank, and a digital system to implement the logic.

5.3. Limitations and sources of uncertainty

The approach showed consistency in peak load reduction, but according to the results, the rebound profile was volatile. The dependency of the rebound on the system response, the initial heating state, the actuator response, and other factors, makes it challenging to identify and predict accurately. The rebound might limit the effectiveness of the DHWPC strategy by creating new peaks. This rebound is due to substation control, not an effect by building thermal mass. Müller and Jansen [32] halved the observed rebound peak through a rebound damping strategy, and a similar strategy could be used as a next step to control rebound peaks.

It should be noted that the effectiveness of the DHWPC is sensitive to the DHW charging flow rate. A reduced charging flow rate would lower the DHW demand peak but extend the charging duration, thereby reducing the coincident SH interruption period and, consequently, the achievable peak load reduction. This trade-off is expected to vary considerably across buildings, depending on substation hydraulic configuration, tank volume, and DHW tapping patterns. A sensitivity study on the charging flow rate would provide deeper insight into the building peak heat demand and would allow a more comprehensive assessment of the strategy's effectiveness across a broader range of installation configurations.

Preprint not peer reviewed

This preprint research paper has not been peer reviewed. Electronic copy available at: https://ssrn.com/abstract=7648871

Another point is component degradation. DHWPC operation increases the frequency of component state changes, valve repositioning, and temperature cycling in the substation. The long-term impact of these increased operation frequencies on valve actuators, pumps, and heat exchangers has not been assessed here and remains a topic for future work.

6. Conclusions

This paper presented a physics-based peak shedding strategy for buildings equipped with DHW tanks, in which the charging of the buffer tank is used as an autonomous trigger to temporarily interrupt the space heating supply, referred to as DHW Peak Compensation (DHWPC) operation. Unlike signal-based demand response, this strategy requires no communication infrastructure, forecasting, dynamic tariffs, or occupant engagement, and can be implemented in existing substation control hardware. The control logic was evaluated through a field experiment in a Danish multi-family residential building over 51 days of operation, covering 228 peak shedding events, and complemented by a district-level simulation study. Additionally, the effectiveness of the strategy on three different building typologies was evaluated.

The main findings are as follows:

1. DHWPC strategy reduced the measured peak substation demand from 218 kW in the reference year to 145 kW in the experiment year, resulting in a 33 % reduction. In addition, the substation peak flow was reduced by 39%, resulting in lower capacity fee for the building.
2. Across all events, the total rebound energy exceeded the total shed energy by about 8 %, and the rebound was considerably more volatile than the shedding.
3. The measurements showed a strong correlation between the rebound peak and the water flow increases after the event compared to before the event. This was caused by the controller reacting strongly to events and opening the valves fully after the events. A gradual increase of the flow temperature setpoint can potentially solve this and reduce the rebound peaks.
4. Thermal comfort was preserved throughout the experiment. Even when the SH was intentionally switched off for up to 3 hours, the indoor temperature sensors did not capture any significant indoor temperature drop.

Preprint not peer reviewed

This preprint research paper has not been peer reviewed. Electronic copy available at: https://ssrn.com/abstract=7648871

5. At the district level, the simulation showed a 32 % reduction in aggregated peak demand and 17% reduction in peak network flow for a district of 50 buildings, with no significant indoor temperature change, confirming that the building-level mechanism can scale to the network level.
6. The peak reduction potential depends strongly on the f_{DHW}. The highest peak load reduction belongs to buildings with neither too high or too low f_{DHW}. The strategy is most effective for buildings with a balanced DHW demand compared with SH demand.

From an economic perspective, the proposed strategy can provide direct financial benefits in district heating markets where tariffs include a capacity-based fixed fee determined by the building's maximum heat demand, such as in Finland, where the fixed fee component of the DH tariff typically includes the peak power or water flow rate [29, 8].

For the implementation of the strategy, there are three main takeaways from this study. First, meaningful peak shedding in district heating can be achieved by an autonomous prioritization rule in the substation at very low capital cost, using hardware that is already in place. Second, the rebound effect is the main technical risk of the strategy. Its volatility means that uncontrolled recovery can locally offset the benefit, so rebound-aware recovery control, such as ramped reactivation of the space heating loop, is a valuable next development step. Third, the existence of a sweet spot in f_{DHW} implies that the conventional multi-family building stock, rather than either the oldest or the energy-efficient buildings, holds the highest potential for DHWPC deployment.

CRediT Author Contribution Statement

Reza Mokhtari: Writing – original draft, Writing – review & editing, Software, Formal analysis, Conceptualization, Methodology, Investigation, Visualization, Validation. **Jan Eric Thorsen**: Writing – review & editing, Conceptualization, Formal analysis. **Rongling Li**: Writing – review & editing, Formal analysis, Conceptualization, Validation, Investigation, Methodology, Resources.

Declaration of Competing Interests

The authors declare no competing interests.

Preprint not peer reviewed

This preprint research paper has not been peer reviewed. Electronic copy available at: https://ssrn.com/abstract=7648871

Data Availability

Data will be made available upon request.

Acknowledgements

The authors acknowledge the European Commission for the ARV project (grant number 101036723), the SEEDS project (grant number 101138211), and the Danish Energy Agency for supporting the Danish delegates participating in IEA EBC Annex 96: "Grid Integrated Control of Buildings" through EUDP (grant number 134251-549133). Additionally, the authors acknowledge Albert Makela from Leanheat and Torben Esbensen from ProjectZero for their support and providing necessary resources for this study.

Appendix A. Baseline Construction Details

For each peak shedding event occurring on date d, the raw Y-day baseline profile is constructed as the element-wise arithmetic mean of the $Y = 10$ most recent non-event days of the same day type (weekday or weekend):

$$P^{\text{raw}}_{\text{SH,baseline}}(t) = \frac{1}{Y} \sum_{k=1}^{Y} P^{k}_{\text{SH}}(t), \qquad t = 1, 2, \ldots, 24h \tag{A.1}$$

where $P^{k}_{\text{SH}}(t)$ is the measured SH power at time t of the k-th selected non-event day. Only days within the heating season (October-April) are included in the selection. To reduce systematic offsets by weather differences between the Y-day average and actual demand conditions on the event day, a multiplicative scaling factor α is applied:

$$\alpha = \frac{\bar{P}_{\text{SH,pre}}}{\bar{P}^{\text{raw}}_{\text{SH,baseline,pre}}} \tag{A.2}$$

where $\bar{P}_{\text{SH,pre}}$ and $\bar{P}^{\text{raw}}_{\text{baseline,SH,pre}}$ are the mean measured and mean raw baseline SH power, respectively, over the $\tau_{\text{pre}} = 30$ min window immediately preceding the event start t_0. The corrected baseline is thus:

$$P_{\text{SH,baseline}}(t) = \alpha \cdot P^{\text{raw}}_{\text{SH,baseline}}(t) \tag{A.3}$$

Preprint not peer reviewed

This preprint research paper has not been peer reviewed. Electronic copy available at: https://ssrn.com/abstract=7648871

Appendix B. Long events

To stress-test the strategy and further study the system behavior, two manual events were designed where SH was manually turned off for a relatively long period and the system response was been evaluated. The results are illustrated in Figure B.14.

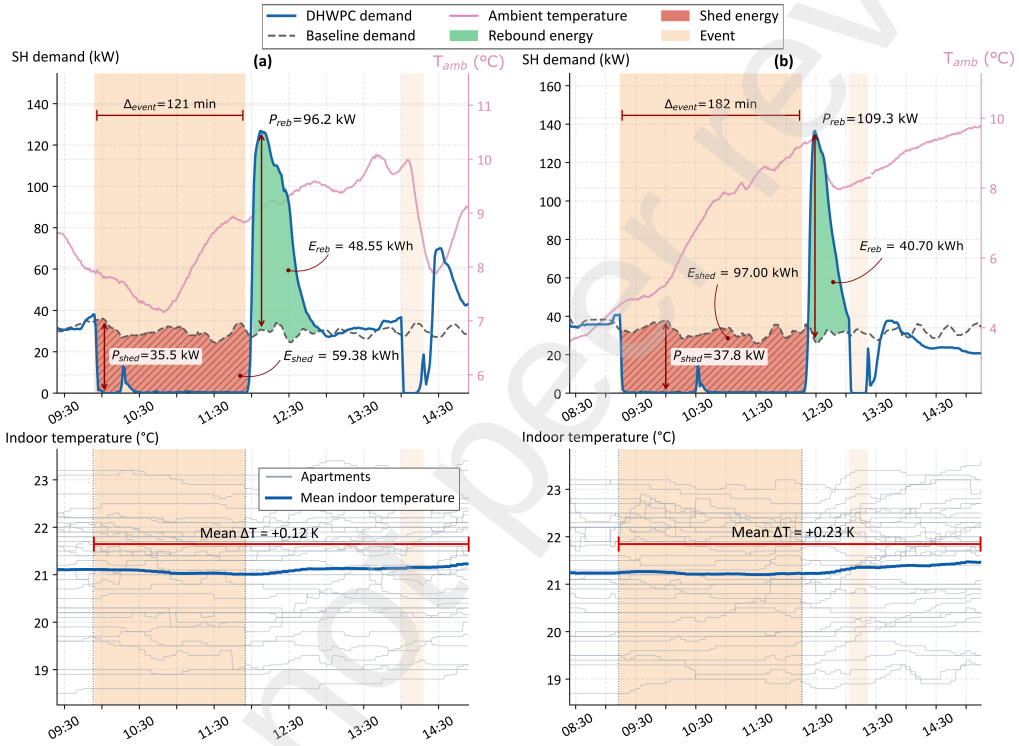


Figure B.14: Heat demand profiles analysis for two intentionally-long events followed by the impact on indoor temperature.

The two events are 121 and 182 minutes, respectively. The rebound power of these two events is much larger than normal DHWPC events, listed in Table 2. However, the E_{reb} is smaller than E_{shed} for both events. The indoor temperature plots show that even though the SH was off for hours, the indoor temperature did not experience any substantial temperature change during and after the events. The average indoor temperature change shows a temperature increase for both events, partly caused by an increase in ambient temperature. All in all, the events indicate that the pilot building has a

Preprint not peer reviewed

This preprint research paper has not been peer reviewed. Electronic copy available at: https://ssrn.com/abstract=7648871

substantial thermal mass to absorb temporary interruptions of SH, allowing DHWPC strategy to be implemented without endangering indoor comfort.

Declaration of generative AI and AI-assisted technologies in the manuscript preparation process

The authors used Claude (Anthropic) to assist with preliminary data analysis and visualization and with Python scripts that connects the co-simulation with FMU of buildings and their substations. The design of the study, field testing, modeling of the buildings and systems, critical thinking, in-depth analysis and knowledge discovery that are presented in the manuscript are done by the authors without the involvement of AI tools. The authors take full responsibility for the content of the article.

References

[1] H. Lund, P. A. Østergaard, P. Sorknæs, S. Nielsen, I. R. Skov, M. Yuan, J. Z. Thellufsen, B. V. Mathiesen, S. M. Benson, A. Jentsch, et al., District heating in clean energy systems, Nature Reviews Clean Technology 1 (8) (2025) 532–546.

[2] H. Ali, A. Volkova, A. Dedov, S. Moser, Rethinking peak load in district heating: Operational insights and techno-economic pathways, Energy Reports 15 (2026) 109061.

[3] R. Egging-Bratseth, H. Kauko, B. R. Knudsen, S. A. Bakke, A. Ettayebi, I. R. Haufe, Seasonal storage and demand side management in district heating systems with demand uncertainty, Applied Energy 285 (2021) 116392.

[4] Z. Ma, M. Lu, X. Yang, M. Hu, A. Prakash, J. Candanedo, S. Tohidi, D. Rovas, S. Katipamula, H. Johra, et al., Delivering building demand flexibility for grid-interactive operation: from perception and cognition to decision, execution, and verification, Applied Energy 426 (2026) 128668.

[5] J. Thorsen, T. Ommen, W. Meesenburg, K. Smith, E. Oliver, EnergyLab Nordhavn (d10.1c): Heat Booster Substation and Circulation Booster for Domestic Hot Water, 2019.

Preprint not peer reviewed

This preprint research paper has not been peer reviewed. Electronic copy available at: https://ssrn.com/abstract=7648871

[6] E. Guelpa, V. Verda, Demand response and other demand side management techniques for district heating: A review, Energy 219 (2021) 119440. doi:10.1016/j.energy.2020.119440.

[7] M. H. Christensen, R. Li, P. Pinson, Demand side management of heat in smart homes: Living-lab experiments, Energy 195 (2020) 116993.

[8] J. Suhonen, J. Jokisalo, R. Kosonen, V. Kauppi, Y. Ju, P. Janßen, Demand response control of space heating in three different building types in finland and germany, Energies 13 (23) (2020) 6296. doi:10.3390/en13236296.

[9] S. Buffa, A. Soppelsa, M. Pipiciello, G. Henze, R. Fedrizzi, Fifth-generation district heating and cooling substations: Demand response with artificial neural network-based model predictive control, Energies 13 (17) (2020) 4339. doi:10.3390/en13174339.

[10] Y. Ju, P. Hiltunen, J. Jokisalo, R. Kosonen, S. Syri, Benefits through space heating and thermal storage with demand response control for a district-heated office building, Buildings 13 (10) (2023) 2670. doi:10.3390/buildings13102670.

[11] Z. Zokirov, The effect of smart heating control on draught in residential buildings (2022).

[12] R. Mokhtari, M. Montazeri, H. Cai, P. Heer, R. Li, Price-responsive control using deep reinforcement learning for heating systems: Simulation and living lab experiment, Energy 337 (2025) 138517. doi:https://doi.org/10.1016/j.energy.2025.138517.

[13] A. Vandermeulen, B. van der Heijde, L. Helsen, Controlling district heating and cooling networks to unlock flexibility: A review, Energy 151 (2018) 103–115. doi:10.1016/j.energy.2018.03.034.

[14] H. Golmohamadi, K. G. Larsen, P. G. Jensen, I. R. Hasrat, Integration of flexibility potentials of district heating systems into electricity markets: A review, Renewable and Sustainable Energy Reviews 159 (2022) 112200. doi:10.1016/j.rser.2022.112200.

Preprint not peer reviewed

This preprint research paper has not been peer reviewed. Electronic copy available at: https://ssrn.com/abstract=7648871

[15] R. Mokhtari, H. Madsen, R. Li, Exploring the impacts of consumer reaction to dynamic heat prices in district heating, Energy and Buildings 347 (2025) 116347. doi:https://doi.org/10.1016/j.enbuild.2025.116347.

[16] Danfoss, Leanheat® monitor, accessed: 2026-07-09 (2026).

[17] M. Wetter, W. Zuo, T. S. Nouidui, X. Pang, Modelica buildings library, in: Journal of Building Performance Simulation, Vol. 7, 2014, pp. 253–270, lBNL Modelica Buildings Library – primary library reference. doi:10.1080/19401493.2013.765506.

[18] A. Marszal-Pomianowska, C. Zhang, M. Pomianowski, P. Heiselberg, K. Gram-Hanssen, A. R. Hansen, Simple methodology to estimate the mean hourly and the daily profiles of domestic hot water demand from hourly total heating readings, Energy and Buildings 184 (2019) 53–64. doi:10.1016/j.enbuild.2018.11.035.

[19] E. Fuentes, L. Arce, J. Salom, A review of domestic hot water consumption profiles for application in systems and buildings energy performance analysis, Renewable and Sustainable Energy Reviews 81 (2018) 1530–1547.

[20] H. Erhorn, H. Erhorn-Kluttig, Selected examples of nearly zero-energy buildings, Report of the Concerted Action EPBD (2014) 65–66.

[21] Y. J. Yu, A. Santos, B. Jørgensen, H. Kazmi, R. Ruusu, A. Hasan, T. Péan, Y. Zhou, Energy in buildings and communities programme. annex 67 energy flexible buildings-control strategies and algorithms for obtaining energy flexibility in buildings, IEA, 2019.

[22] K. Coughlin, M. A. Piette, C. Goldman, S. Kiliccote, Statistical analysis of baseline load models for non-residential buildings, Energy and Buildings 41 (4) (2009) 374–381.

[23] G. Reynders, J. Diriken, D. Saelens, Generic characterization method for energy flexibility: Applied to structural thermal storage in residential buildings, Applied Energy 198 (2017) 192–202. doi:10.1016/j.apenergy.2017.04.061.

Preprint not peer reviewed

This preprint research paper has not been peer reviewed. Electronic copy available at: https://ssrn.com/abstract=7648871

[24] K. Zhang, M. Kummert, Evaluating the impact of thermostat control strategies on the energy flexibility of residential buildings for space heating, Building Simulation 14 (2021) 1439–1452. doi:10.1007/s12273-020-0751-x.

[25] ASHRAE, Ashrae guideline 14-2014: Measurement of energy, demand, and water savings, Tech. rep., American Society of Heating, Refrigerating and Air-Conditioning Engineers, Atlanta, GA, USA (2014).

[26] J. Granderson, P. N. Price, D. Jump, N. Addy, M. D. Sohn, Automated measurement and verification: Performance of public domain whole-building electric baseline models, Applied Energy 144 (2015) 106–113. doi:10.1016/j.apenergy.2015.01.026.

[27] J. Le Dréau, P. Heiselberg, Energy flexibility of residential buildings using short term heat storage in the thermal mass, Energy 111 (2016) 991–1002. doi:10.1016/j.energy.2016.05.076.

[28] A. Arteconi, N. J. Hewitt, F. Polonara, State of the art of thermal storage for demand-side management, Applied Energy 93 (2012) 371–389. doi:10.1016/j.apenergy.2011.12.045.

[29] P. Ala-Kotila, T. Vainio, J. Heinonen, Demand response in district heating market—results of the field tests in student apartment buildings, Smart Cities 3 (2) (2020) 157–171. doi:10.3390/smartcities3020009.

[30] R. G. Junker, A. G. Azar, R. A. Lopes, K. B. Lindberg, G. Reynders, R. Relan, H. Madsen, Characterizing the energy flexibility of buildings and districts, Applied Energy 225 (2018) 175–182. doi:10.1016/j.apenergy.2018.05.037.

[31] Y. Ju, J. Lindholm, M. Verbeck, J. Jokisalo, R. Kosonen, P. Janßen, Y. Li, H. Schäfers, N. Nord, Cost savings and co2 emissions reduction potential in the german district heating system with demand response, Science and Technology for the Built Environment 28 (2) (2022) 255–274. doi:10.1080/23744731.2021.2018875.

[32] F. L. Müller, B. Jansen, Large-scale demonstration of precise demand response provided by residential heat pumps, Applied Energy 239 (2019) 836–845. doi:10.1016/j.apenergy.2019.01.202.

Preprint not peer reviewed

This preprint research paper has not been peer reviewed. Electronic copy available at: https://ssrn.com/abstract=7648871